Electrical Power and Energy Systems 103 (2018) 537–544

Contents lists available at ScienceDirect

Electrical Power and Energy Systems

journal homepage: www.elsevier.com/locate/ijepes

Model predictive control design for DC-DC converters applied to a photovoltaic system

Ahmad Dehghanzadeh[a,*], Gholamreza Farahani[a], Hani Vahedi[c], Kamal Al-Haddad[b]

[a] Iranian Research Organization for Science and Technology, Tehran, Iran
[b] École de Technologie Supérieure, Montreal, Canada
[c] Ossiaco Inc., Montreal, Canada

ARTICLE INFO

Keywords:
Photovoltaic (PV)
Incremental conductance
Model predictive control (MPC)
Continuous control set (CCS)

ABSTRACT

A continuous control set model predictive control (CCS-MPC) is designed for a DC-DC buck converter used in maximum power point tracking (MPPT) of a photovoltaic (PV) module. A modified incremental conductance (m-INC) algorithm is used for MPP determination as a reference signal for CCS-MPC. The small-signal model of the PV system is adaptively obtained around MPP through linearization of its average model. The predictive control is designed and applied to a PV system using an online optimization of the cost function including the discretized present and future states. The performance of the proposed m-INC CCS-MPC is evaluated by simulation study that indicates better performance in terms of transient and disturbance rejection compared to conventional PI controller. Finally, the applicability of the proposed m-INC CCS-MPC strategy is assessed with outdoor experimental results and the associated practical advantages against finite control set (FCS) MPC are discussed.

1. Introduction

Despite the reduction of solar installation cost by a ratio of 10 during the last 20 years, still conversion efficiency of PV panels remains an important parameter to take into account when designing solar system for residential applications [1]. Therefore, an efficient MPPT algorithm plays a key role to harvest optimum available power especially in large solar installations. Several MPPT algorithms have been elaborated in the literature. Among them, perturb and observe (P&O) and incremental conductance (INC) are practically favorable as the awareness of PV panel characteristics is not required. Moreover, their procedures to find MPP are independent of temperature and irradiation values that their measurements need expensive sensors [2,3]. Principally, P&O and INC are inherently perturbative methods that produce reference voltage or current to be tracked by a subsequent controller. The PI controller has been widely used in MPPT operations [4,5]; however, continuous evolution in microprocessor technology facilitates implementing advanced controllers for efficiency enhancement of MPPT algorithm. The ability of Fuzzy logic [6,7], neural network [8] and genetic algorithm [9] has been investigated in MPPT modules. This paper deals with predictive technique that is lately well adopted for various applications. Indeed, model predictive controller (MPC) is a competitive alternative to address the growing industrial concerns regarding to performance and efficiency issues. It can also formulate inherent nonlinearity in power electronic systems with operational constraints. Moreover, its realization in state matrix can be easily extended to multivariable systems [10]. Basically, MPC solves an optimization problem within a moving time horizon in order to generate future actions for optimal operation of a plant. In fact, at each sampling time, MPC reconstructs instant operating model of the plant, predicts future states and optimizes current dynamic while taking into account the future states. Real time modification is a desirable property in practice that can compensate inevitable modeling errors [11].

In power electronics, MPC were emerged with finite control set (FCS) appearance. Actually the pulse activation nature of switching converters allowed defining FCS-MPC that evaluates cost function in only possible switching states. A low complexity optimization algorithm is solved and simply the minimum cost is selected among predetermined states at each sampling time. FCS-MPC has been investigated in most applications of power converters [12–14], and especially in PV systems [15–18]. Despite numerous reports in this area, the applicability of FCS-MPC is yet a challenge. It works with variable switching frequency which leads to a widespread harmonics spectrum for voltage/current waveforms. This is a fundamental limitation that hinders filter design [19,20], increases switching losses, makes unwanted resonances, and consequently reduces system

* Corresponding author at: Department of Electrical Engineering and Information Technology, Iranian Research Organization for Science and Technology, Sh. Ehsani Rad St., Enqelab St., Parsa Sq., Ahmadabad Mostoufi Rd., Azadegan Highway, P.O. Box 3353-5111, Tehran 3353136846, Iran.
E-mail addresses: a.dehghanzadeh@irost.ir (A. Dehghanzadeh), farahani.gh@irost.ir (G. Farahani), hani.vahedi@ieee.org (H. Vahedi), kamal.al-haddad@etsmtl.ca (K. Al-Haddad).

https://doi.org/10.1016/j.ijepes.2018.05.004
Received 19 November 2017; Received in revised form 27 April 2018; Accepted 9 May 2018

performance in terms of power quality [21]. However, the switching frequency could be regulated by including some more terms in the cost function, it would add the complexity and consequently the computation burden to the FCS-MPCs while distracting control effort from main target of the reference tracking [22,23]. Moreover, none-zero steady state error is reported in [24,25]. Furthermore, the computational burden increases exponentially in multilevel converters with high number of switching states [26].

To address these existing issues of FCS-MPC, this paper formulates continuous control set (CCS) MPC in a PV system supplying DC bus through a buck converter. The CCS-MPC strategy benefits from the average model of the systems and then uses a modulator to ignite the converter switches resulting a fixed switching frequency. The relatively high accuracy of the models for power converters is an opportunity to define complex performance criteria introduced by CCS-MPC to achieve the desired dynamic. Besides, an integrator is augmented in the proposed MPC design in order to comply with steady state requirements. To evaluate the efficiency of the proposed controller, the performances of CCS-MPC is compared to the conventional PI controller while both are using m-INC as MPPT algorithm.

The rest of this paper is organized as follows: the overall configuration of the PV system is demonstrated in section II. The switch model of the PV system is acquired in bilinear compact form. Afterwards, the average model is derived from the switch model to have continuous manipulating variable for the proposed controller. In Section 3, the INC method is modified and elaborated (called m-INC) in order to find real time MPP as the reference signal for CCS-MPC. In Section 4, the methodology of CCS-MPC approach is explained in three stages. The operating point of the system is calculated in first stage. Subsequently, the nonlinear average model of the system is linearized around the operating point that yields small-signal model. Moreover, a discretization is done in this stage for DSP implementation. Secondly, using output and states variations, an augmented system is developed to benefit from an integral control action for steady state purposes. Also, the predicted vectors of states and output in the form of augmented systems are obtained. In the third stage, the optimum duty cycle is generated by real time optimization of a cost function, which is modulated through a PWM block. The performance of the proposed MPC is examined by modeling PV panel and converter in SimPowerSystems of MATLAB software in Section 5. The practical test results of PV set-up are presented and discussed in Section 6 to validate the theoretical and simulation studies.

2. PV system modeling

A practical photovoltaic system is shown in Fig. 1, where power is delivered to an energy storage system through a buck converter. The buck converter is employed in order to control the operating point of PV panel at MPP and it may be replaced with boost or buck-boost converters depending on the specific application. In this PV system, the output voltage is kept constant at V_{DC} by a battery or by having a DC to AC converter feeding power to the grid. Moreover, for supplying DC distribution system, an additional controlled converter may be used to stabilize output DC voltage. Furthermore, in grid-connected PV systems, an independently controlled inverter may be used to provide AC voltage. It is worthwhile to mention that in dark condition, the voltage of PV panel may be less than V_{DC}, so if there is no blocking diode, the battery would flow a current with opposite direction that discharges the battery. As blocking diodes are usually included in the construction of PV panels, no more diodes are considered in Fig. 1. Moreover, the battery voltage V_{DC} is known and measured only for rejecting disturbances on DC bus voltage.

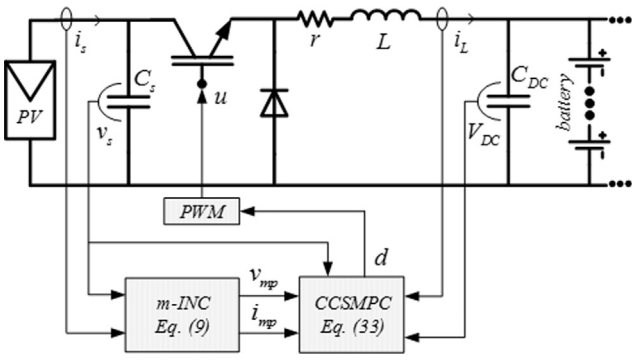

Fig. 1. Schematic of a PV system with block diagram of the proposed control structure.

The converter is driven by switching signal $u(t)$ generated through PWM. The signal $u(t)$ is defined in Eq. (1) with period T and duty ratio d.

$$u(t) = \begin{cases} 1 & 0 \leqslant t < dT \\ 0 & dT \leqslant t \leqslant T \end{cases} u(t-T) = u(t)\ \forall\ t \tag{1}$$

Applying the Kirchhoff's laws on the circuit of Fig. 1 distinctly in two switching states 0 and 1, a single unified model in a compact form can be presented by Eq. (2). This model is called switched model as it describes switching dynamics of power electronic converters.

$$\begin{cases} -i_s(t) + C_s\frac{dv_s(t)}{dt} + u(t)i_L(t) = 0 \\ -u(t)v_s(t) + ri_L + L\frac{di_L(t)}{dt} + V_{dc} = 0 \end{cases} \tag{2}$$

In control theory, it is desired to work with a continuous manipulating signal than two switching states of $u(t)$ [27]. Using definitions in Eqs. (3)–(5), averaging technique is employed to transform the discontinuous model of Eq. (2) to the continuous model of Eq. (6) for CCS-MPC algorithm. The symbol x_0 signifies average operation on x; however, the previous symbols are used again in Eq. (6) for simplicity, but duty ratio $d(t)$ is substituted as the average variable of $u(t)$ in sliding period of T.

$$\langle x(t)_0\rangle(t) = \frac{1}{T}\int_{t-T}^{t} x(\tau)d\tau \tag{3}$$

$$\left\langle \frac{dx(t)}{dt} \right\rangle_0 (t) = \frac{d}{dt}\langle x(t)\rangle_0 \tag{4}$$

$$\langle x(t)u(t)\rangle_0(t) \approx \langle x(t)\rangle_0(t)\langle u(t)\rangle_0(t) \tag{5}$$

$$\begin{cases} \frac{dv_s(t)}{dt} = \frac{1}{C_s}(i_s(t) - d(t)i_L(t)) \\ \frac{di_L(t)}{dt} = \frac{1}{L}(-ri_L(t) + d(t)v_s(t) - V_{dc}) \end{cases} \tag{6}$$

The system of Eq. (6) is not an exact model of the PV system, however, adequately represents low frequency behavior of signals while neglecting high frequency components caused by switching action. It is a natural practice since high-frequency switching phenomena are parasitic contents in most power electronics applications that are eliminated by filters [28].

2.1. MPPT algorithm

In this section, INC with some modifications is used to determine the reference signals for MPC [2]. Simply, the output power of PV panel is described as:

$$p_s(t) = v_s(t)i_s(t) \tag{7}$$

The slope of power signal with respect to the output voltage of the panel can be stated as Eq. (8), where g and dg are conductance and differential conductance, respectively.

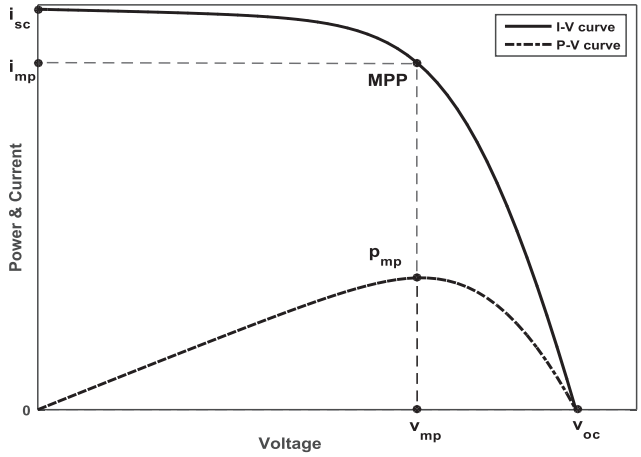

Fig. 2. I-V and P-V characteristics of a PV panel.

$$\frac{dp_s(t)}{dv_s(t)} = v_s(t)\left(\frac{i_s(t)}{v_s(t)} + \frac{di_s(t)}{dv_s(t)}\right) = v_s(t)(g(t) + dg(t)) \tag{8}$$

The sign of the slope as given in Eq. (8) intuitively determines the current operating point of solar panels in respect to the MPP over P-V curve. Fig. 2 shows the positions of short circuit current (i_{sc}), open circuit voltage (v_{oc}), maximum power point (MPP), voltage at MPP (v_{mp}), and current at MPP (i_{mp}). It is obvious that the slope of P-V curve is positive at left side and negative at right side of MPP. Thus, by measuring v_s and i_s, the variables g and dg would be calculated that yield MPP in the form of Eq. (9). The parameters of V_{inc} and I_{inc} are chosen based on the trade-off between transient speed and inherent steady-state oscillation of INC.

$$\begin{cases} v_{mp}(t) = v_s(t) + V_{inc}sign(g(t) + dg(t)) \\ i_{mp}(t) = i_s(t) - I_{inc}sign(g(t) + dg(t)) \end{cases} \tag{9}$$

Two modifications are considered for the traditional INC algorithm. Firstly, current reference is also included as the reference signal in order to match the CCS-MPC equations requirements. Secondly, the perturbations of V_{inc} and I_{inc} are exerted to the instant voltage and current of PV panel, but not to the previous sample of reference signal; this can improve the performance of MPPT to find the right direction and move with larger step toward MPP over P-V curve during rapid change of irradiation. The procedure of m-INC is clarified in the flowchart of Fig. 3, where $k-1$ indicates the values at previous sample and k shows the instant measured values. In fact, this procedure determines desired operating point of the PV system at maximum available power.

3. CCS-MPC design approach

3.1. Discrete small-signal model

Since v_{mp} and i_{mp} have been already determined in previous section, the desired operating points for i_L and d can be obtained by making derivatives of the system equal to zero in Eqs. (6) through (10) and (11):

$$d_{mp}(t) = \frac{V_{dc} + \sqrt{V_{dc}^2 + 4rv_{mp}(t)i_{mp}(t)}}{2v_{mp}(t)} \tag{10}$$

$$i_{Lmp}(t) = \frac{i_{mp}(t)}{d_{mp}(t)} \tag{11}$$

Knowing the nominal states and input variable, the nonlinear system of Eq. (6) can be linearized using Taylor series expansion [29]. The linear small-signal model of the PV system is achieved as Eq. (12). The state vector of the small-signal model is defined as $x = [v_s \quad i_L]^T$.

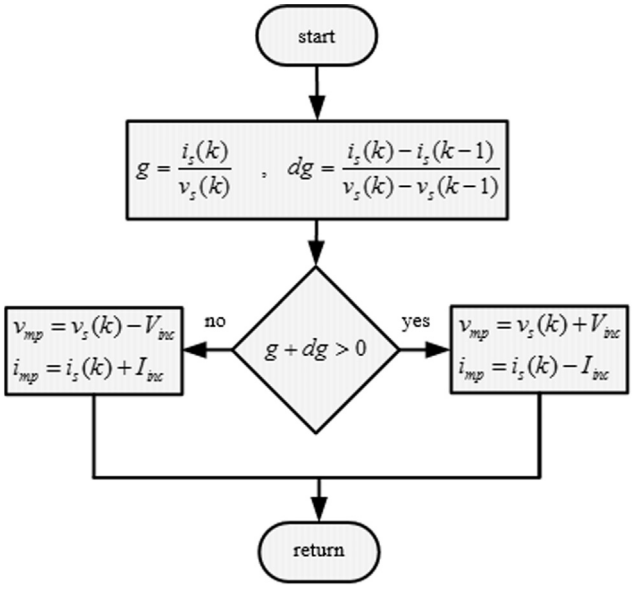

Fig. 3. The procedure of m-INC to determine reference signals for CCS-MPC.

Obviously, the signals in Eq. (12) are variation of the initial signals of v_s, i_L and d. Worth mentioning that the initial notations are preserved only for the convenient understanding.

$$\begin{cases} \frac{dx(t)}{dt} = A_c(t)x(t) + B_c(t)d(t) \\ y(t) = C_c(t)x(t) \end{cases} \tag{12}$$

where:

$$\begin{cases} A_c = \begin{bmatrix} \frac{dg_{mp}(t)}{C_s} & -\frac{d_{mp}(t)}{C_s} \\ \frac{d_{mp}(t)}{L} & -\frac{R}{L} \end{bmatrix}, B_c = \begin{bmatrix} -\frac{i_{Lmp}(t)}{C_s} \\ \frac{v_{mp}(t)}{L} \end{bmatrix} \\ C_c = [1 \quad 0] \end{cases} \tag{13}$$

As Eq. (8) is equal to zero at MPP, the value of dg_{mp} in Eq. (13) is evaluated as:

$$dg_{mp}(t) = \frac{di_s(t)}{dv_s(t)}\bigg|_{mp} = -\frac{i_{mp}(t)}{v_{mp}(t)} \tag{14}$$

For DSP implementation of MPC, the discretized form of small-signal model is required that is described as:

$$\begin{cases} x(k+1) = A_d x(k) + B_d d(k) \\ y(k) = C_d x(k) \end{cases} \tag{15}$$

where the discrete-time state space matrices can be obtained through Eq. (16). These matrices are time variant; however their values are supposed to be constant within each sampling time T_s.

$$\begin{cases} A_d = \exp(A_c T_s), B_d = \int_0^{T_s} \exp(A_c \tau) B_c d\tau \\ C_d = C_c \end{cases} \tag{16}$$

3.2. Predictive variables

In this subsection, the predicted states and output of the PV system are extracted based on discrete small-signal model of the PV system. To address steady-state tracking purposes, a new state vector of Eq. (17) is considered in which an integrator is augmented [11].

$$x_a(k) = [\Delta x(k)^T \quad y(k)]^T \tag{17}$$

where

$$\Delta x(k) = x(k) - x(k-1) \tag{18}$$

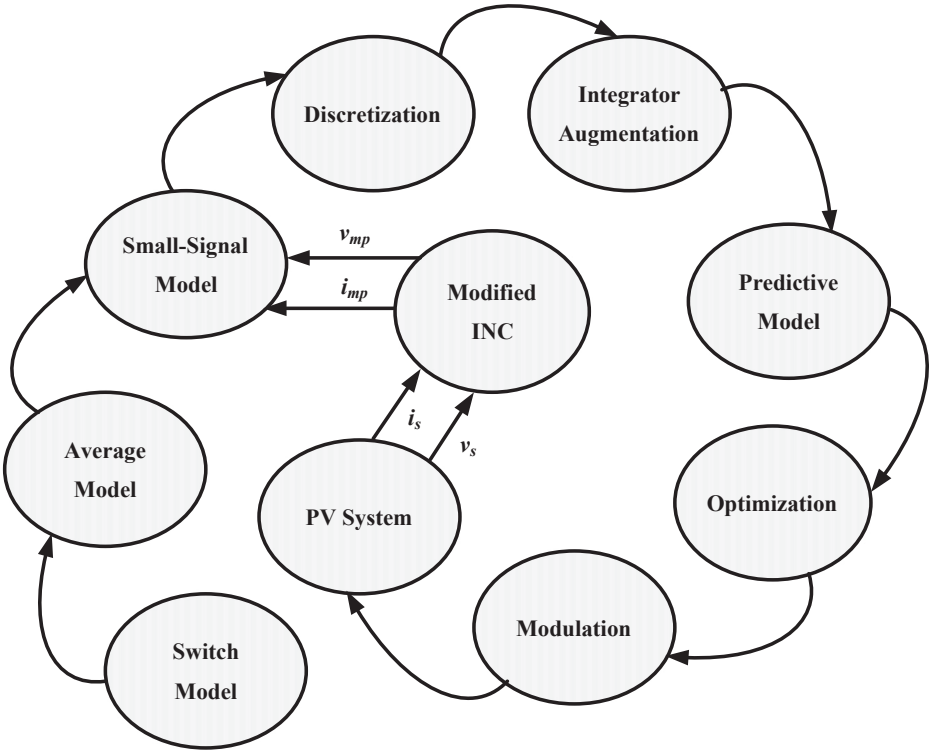

Fig. 4. The schematic of the proposed m-INC CCS-MPC methodology for MPPT of a PV system.

Hence the augmented model of the PV system is represented as:

$$\begin{cases} x_a(k+1) = A_a x_a(k) + B_a \Delta d(k) \\ y(k) = C_a x_a(k) \end{cases} \tag{19}$$

where

$$\Delta d(k) = d(k) - d(k-1) \tag{20}$$

and

$$\begin{cases} A_a = \begin{bmatrix} A_d & 0 \\ C_d A_d & 1 \end{bmatrix}, B_a = \begin{bmatrix} B_d \\ C_d B_d \end{bmatrix} \\ C_a = [0 \quad 0 \quad 1] \end{cases} \tag{21}$$

Using Eq. (19), the predicted augmented states and output can be obtained by Eqs. (22) and (23); where N_p is called prediction horizon, which determines the numbers of future states, required for optimization, and N_c is control horizon in which future control actions are produced.

$$\begin{cases} x_a(k+2) = A_a^2 x_a(k) + A_a B \Delta d(k) + B \Delta d(k+1) \\ \vdots \\ x_a(k+N_p) = A_a^{N_p} x_a(k) + \\ A_a^{N_p-1} B \Delta d(k) + A_a^{N_p-2} B \Delta d(k+1) + \\ \cdots + A_a^{N_p-N_c} B \Delta d(k+N_c-1) \end{cases} \tag{22}$$

$$y(k+N_p) = C_a x_a(k+N_p) \tag{23}$$

By defining the vectors of Eqs. (24), all the predicted states and output variables are described in a compact form of Eq. (25).

$$\begin{cases} Y = [y(k+1) \quad y(k+2) \quad \ldots \quad y(k+N_p)]^T \\ \Delta D = [\Delta d(k) \quad \Delta d(k+1) \quad \ldots \quad \Delta d(k+N_c-1)]^T \end{cases} \tag{24}$$

$$Y = F x_a(k) + \Phi \Delta D \tag{25}$$

where

$$F = [C_a A_a \quad C_a A_a^2 \quad \ldots \quad C_a A_a^{N_p}]^T \tag{26}$$

$$\Phi = \begin{bmatrix} C_a B_a & 0 & \cdots & 0 \\ C_a A_a B_a & C_a B_a & \cdots & 0 \\ \vdots & \vdots & \cdots & 0 \\ C_a A_a^{N_p-1} B_a & C_a A_a^{N_p-2} B_a & \cdots & C_a A_a^{N_p-N_c} B_a \end{bmatrix} \tag{27}$$

3.3. Optimization

To control the output voltage of PV panel at MPP, the reference signal of MPC is considered as v_{mp} in whole prediction horizon that is defined by R_s as:

$$R_s = [1 \quad 1 \quad \cdots \quad 1]^T v_{mp} \tag{28}$$

The objective of the MPC is minimizing the error between predicted output variables and reference vector of R_s, while some consideration may be given to the amplitude of ΔD. Thus, the cost function of MPC is generally expressed as:

$$J = (R_s - Y)^T (R_s - Y) + \Delta D^T R_w \Delta D \tag{29}$$

where R_w is a weighting factor described by a diagonal matrix of:

$$R_w = r_w I_{N_c \times N_c} \tag{30}$$

The value of r_w determines how much one can pay attention to ΔD; in fact, $r_w = 0$ means that the amount of ΔD is not the concern and the only objective is to make the error $(R_s - Y)^T (R_s - Y)$ as small as possible. The same weighting factor of $r_w = 0.001$ is considered over the control

Table 1
PV system specification in this study.

Source capacitance (C_s)	150 μF
Inductor (r, L)	1 mΩ·0.5 mH
DC bus capacitance (C_{dc})	150 μF
Battery voltage (V_{dc})	≈ 12 V
Load	40 Ω
Switching frequency	5 kHz
Sampling time (T_s)	20 μs

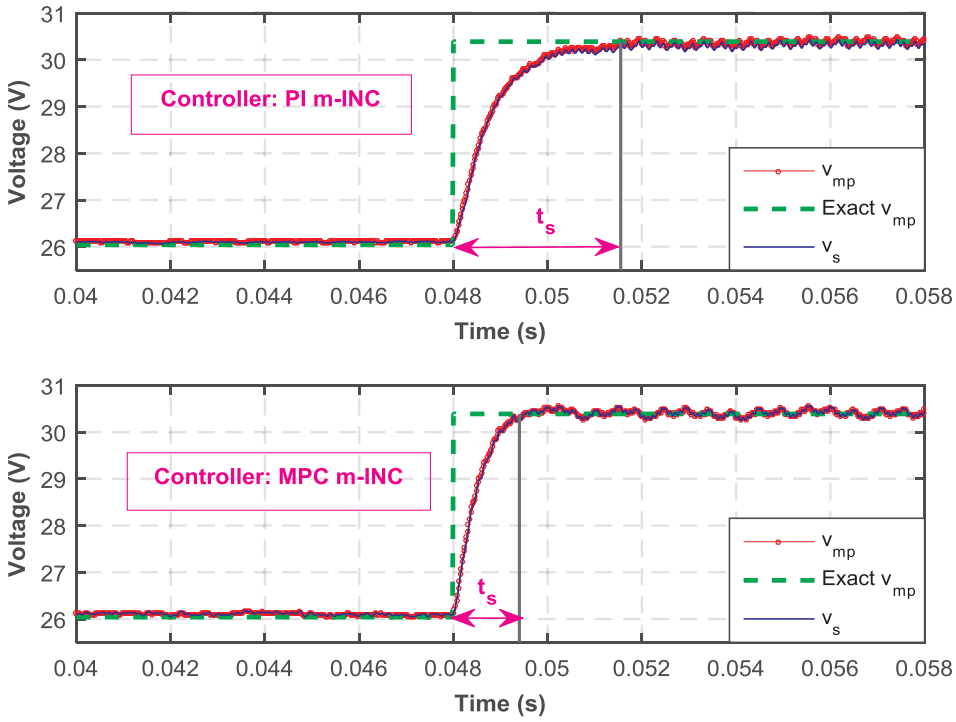

Fig. 5. The closed loop performance of the controllers during an abrupt change of irradiation for PI and CCS-MPC.

horizon. Using Eq. (25), the cost function of Eq. (29) can be restated as:

$$J = (R_s - Fx_a(k))^T(R_s - Fx_a(k)) - 2\Delta D^T\Phi^T(R_s - Fx_a(k)) + \Delta D^T(\Phi^T\Phi + R_w)\Delta D \quad (31)$$

The minimum value of J can then be easily acquired by a derivative respect to the ΔD:

$$\frac{\partial J}{\partial \Delta D} = -2\Phi^T(R_s - Fx_a(k)) + 2(\Phi^T\Phi + R_w)\Delta D \quad (32)$$

Eventually, the optimum variation of duty cycle is resulted in:

$$\Delta D = (\Phi^T\Phi + R_w)^{-1}\Phi^T(R_s - Fx_a(k)) \quad (33)$$

Afterwards, the control sequence is computed within control horizon that the only first action is sent to the duty cycle. The flowchart of the proposed predictive controller operating along with m-INC is illustrated in Fig. 4.

4. Simulation study

To evaluate the effectiveness of the proposed method for controller design, the circuit shown in Fig. 1 is simulated in SimPowerSystems toolbox of Matlab. The values of the circuit elements are listed in Table 1. A two-diode model with parasitic series and parallel resistances is used as equivalent circuit of PV panel. Based on the mathematical model of PV panel and environmental changes, the exact voltage and current at MPP are also calculated so that the accuracy of the proposed MPPT method could be examined. The electronic model of the PV module and its analytic calculation of exact MPP in this paper comply with results recently reported in [30,31].

The proposed MPC is compared to PI controller in an abrupt change in irradiation from 200 to 800 W/m^2. To do so, the m-INC block calculates real time v_{mp} and i_{mp} using the actual voltage and current measured at the PV panel. The regulating parameters of V_{inc} and I_{inc} for m-INC are selected based on try and error regarding two factors of speed and steady-state oscillation around MPP. The instant reference generated by m-INC is tracked by both of the PI and CCS-MPC controllers in order to compare their performance for MPPT action. The PI design process is based on the procedure explained in [32]. The output voltage of the PV panel for both cases of PI and CCS-MPC are shown in Fig. 5. To verify the accuracy of m-INC for MPPT, the exact v_{mp} and i_{mp} are calculated based on the characteristic of the PV panel that are shown in Fig. 5 with dashed green[1] line. Based on the PV panel model, the exact v_{mp} are obtained as 26.04 V and 30.38 V for the irradiation 200 and 800 W/m^2 respectively. The MPC reference signal computed by m-INC is shown with dotted red line and the voltage of the PV panel with blue line. It is worth to mention that the same filters are used to filter the high frequency components of the voltage and current from the PV panel in both conditions.

As Fig. 5 shows, both controllers could track the new equilibrium point during a few milliseconds. The capability to reach the exact V_{mp} proves the consistency of the controllers and the modified MPPT algorithm of m-INC. Since an augmented integrator is used for CCS-MPC, it approximately represents a non-zero steady state error that is analogous with PI controller performance in steady state. The persistent oscillations around the equilibrium points arise from the perturbation mechanism of m-INC to find the real time maximum power point. To measure the transient performance, the settling time of the controllers can be measured as the time at which the voltage waveform has entered and remained within a band around the exact V_{mp}. The value of the settling time is calculated 3.5 ms for PI and 1.4 ms for CSS-MPC. This signifies that the proposed predictive controller is at least two times faster than the conventional PI controller while operating at the same switching frequency.

The performance of the proposed controller and PI is also compared in response to the sinusoidal irradiation depicted in Fig. 6c. The output current of PV panel is plotted in Fig. 6 for both controllers. As it is clear in Fig. 6a and b, the photocurrent of the PV panel is straightly dependent to the irradiation. It seems both controllers could provide the maximum available power but for an appropriate evaluation, a disturbance is applied to PV system as DC bus voltage step change at 2.5 s.

[1] For interpretation of color in Fig. 5, the reader is referred to the web version of this article.

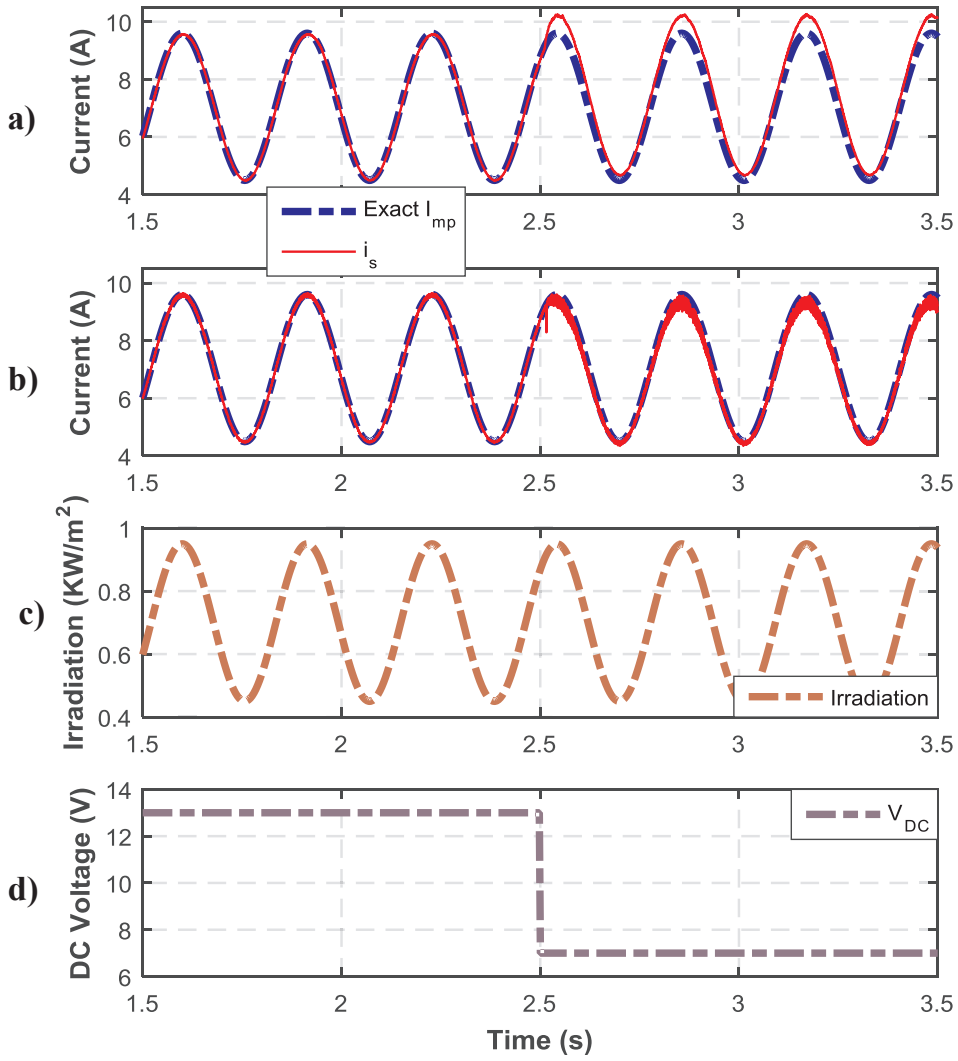

Fig. 6. The closed loop performance of the controllers during a sinusoidal irradiation and a step disturbance in DC link voltage. (a) PI controller, (b) CCS-MPC, (c) irradiation waveform and (d) DC bus voltage.

Table 2
JKM265P poly-crystalline PV module characteristics at stc.

V_{oc}	38.6 V
I_{sc}	9.03 A
V_{mp}	31.4 V
I_{mp}	8.44 A

As it was expected, the PI controller failed to track the current associated to maximum power since it does not use the model of the system. Although PI controllers may be designed in a manner that could reject some particular step disturbances in linear systems, it may totally lose its effectivity within such a complicated nonlinear system. On the contrary, as noted in section I, the modeling of power electronic systems is straightforward with relatively high precision. Hence, it allows defining advanced controller like CCS-MPC to enhance the tracking dynamic for applications in which the energy efficiency is physically low. Fig. 6b shows the proposed controller actively reacts to the voltage disturbance in DC link; as a result, the PV system could rapidly recover the maximum available power. Besides, the sum square error (SSE) are computed as 9535 and 1723 respectively for PI and CCS-MPC controllers from 1.5 s up to 3.5 s that shows much more efficiency of the proposed controller in general applications of PV systems.

5. Experimental results

A JKM265P poly-crystalline PV module is used in the experiment that consists of 60(6 × 10) cells. The nominal power of the panel is 265 W at standard test condition (STC). Specifically STC signifies the irradiation of 1000 W/m^2 at the airmass (AM) of 1.5 and temperature of 25 °C. Since the dimensions of the panel is 1650 × 992 × 40 mm, its efficiency can be calculated as 16.19% at STC. The specifications of the module at STC are listed in Table 2.

To conduct the practical tests, the PV panel has been connected to the batteries through a DC-DC buck converter based on the schematic shown in Fig. 1. The capacitor C_s mounted at the PV panel output is for control purposes. In addition, it filters the high switching frequency components injected from the converter side. The designed algorithm of CCS-MPC has been implemented on a dSpace 1103 real-time controller to generate associate switching pulses. A minimum 20us sampling time is reached for the calculations of the proposed controller. All the voltage/current feedback signals have been provided through OpalRT high bandwidth voltage/current measurement box. System parameters used in practical tests are same as the simulation study listed in Table 1. The experimental set up is shown in Fig. 7 where the PV panel is mounted on a wooden structure in outdoor area. The generated photocurrent is transmitted with a cable to the converter and measurement system inside the building.

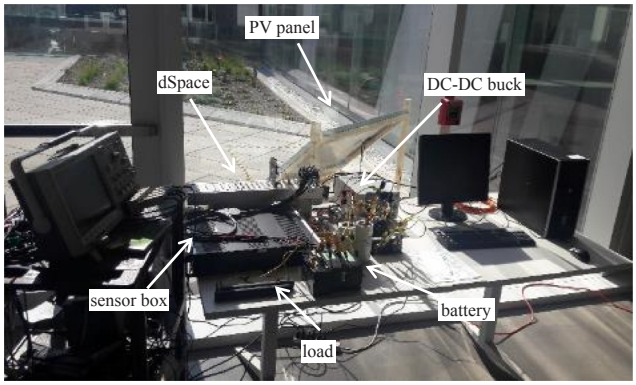

Fig. 7. Experimental set-up for CCS-MPC in outdoor implementation of the PV system.

The experimental tests have been performed during a windy condition followed by a smooth weather. The comparison of CCS-MPC and PI controller is impossible in practice since the same environmental conditions cannot be repeated for the second method. As illustrated in Fig. 8, the voltage, current and power of the PV panel have been captured when CCS-MPC implemented to the aforementioned PV system within a time window of 24 minutes. The red dotted line indicates the reference signal produced by m-INC block. Obviously, the control approach in this paper succeeded to rapidly track MPP in inevitable change of irradiation at the first 800 s of Fig. 8. It is well known that i_{mp} is more dependent to irradiation, hence its variation is much more than v_{mp}. For the rest of the experiment, the irradiation became approximately constant; a zoomed capture of constant irradiation area is also demonstrated indicating the fact that the controller and m-INC find the MPP with about 99.52% efficiency in harvested power. It is worth to mention that in outdoor PV experiments, the efficiency of MPPT and controller could not be exactly determined since the exact MPP is not available. The exact MPP requires the precise physical model of the PV panel that needs real data in a vast range of environmental conditions; manufactures provide only the real data at STC. Moreover, to truly find MPP, the temperature and irradiation measurements are necessary that are not practical in commercial use. Hence, efficiency comparison could not be performed with available reports in literature because all of them evaluated their control methods using PV simulators and not a real panel.

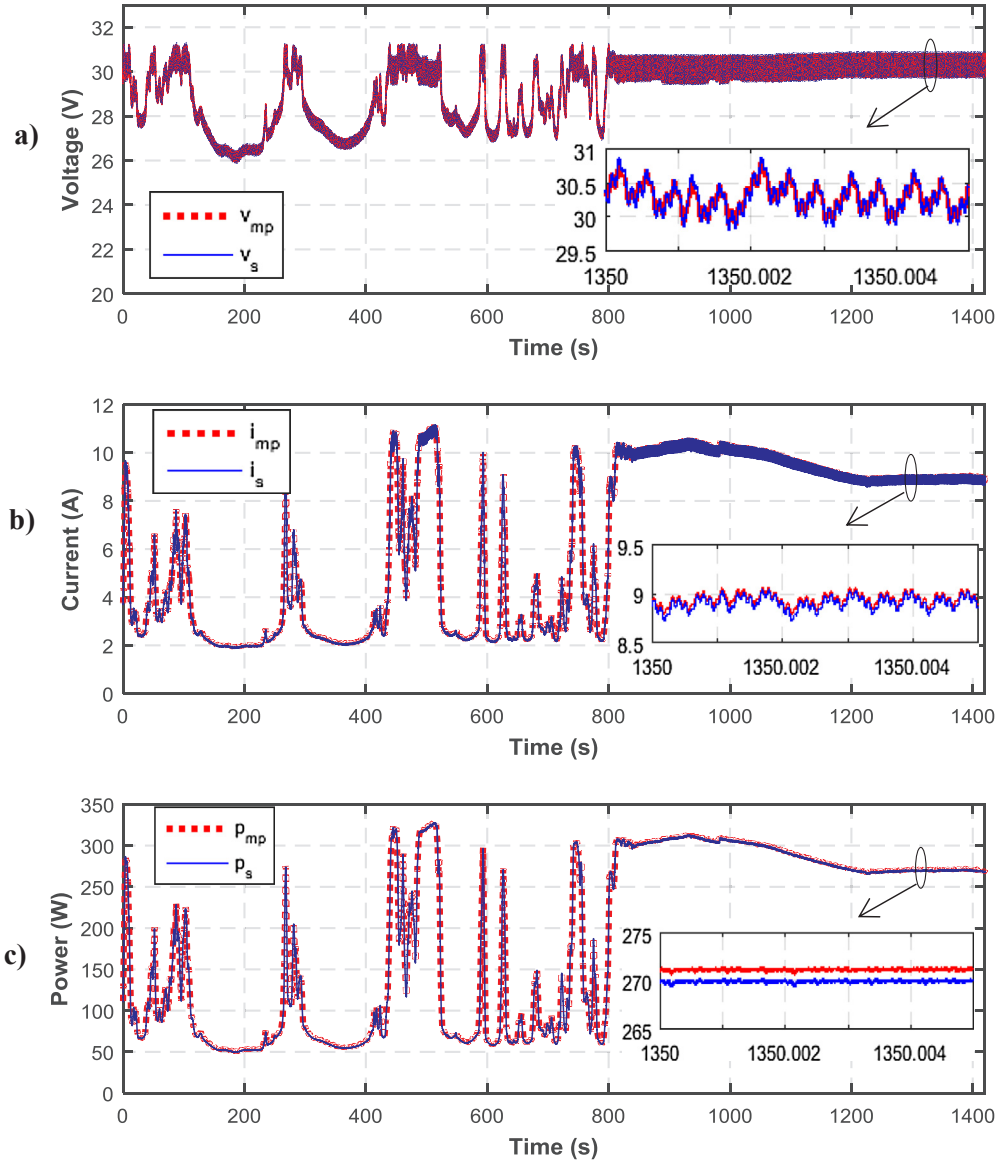

Fig. 8. Experimental results for CCS-MPC. (a) The voltage, (b) current and (c) power of the PV panel.

It is significant to highlight the fact that a long prediction horizon improves the PV system stability in comparison with short prediction horizon [13]. The implementation of FCS-MPC has been mostly limited to the unit prediction horizon in the applications reported in the literature since the computational efficiency of FCS-MPC algorithms is extremely reduced by increasing prediction horizon. Actually, FCS-MPC evaluates a cost function in all possible switching states; so by increasing the prediction horizon, the required calculations grow exponentially. It would be worse in advanced converters (such as multilevel topologies) with high amount of computations due to increased number of semiconductors and consequently having numerous switching states. On the contrary, the optimization process of CCS-MPC is not severely affected by the length of prediction horizon. This is practically promising to have a long prediction horizon especially during the abrupt changes in the irradiation at which the MPPT should asymptotically track the maximum power. Moreover, neglecting the high computation burden imposing the FCS-MPC optimization algorithm, it is not practically feasible because the value of the PV panel voltage is not available at t_{k+1} for the k bigger than 1. In fact, the discretized form of the switch model is used for FCS-MPC; so the one-step-ahead voltage can be simply calculated by the discretized form of Eq. (2). However, the next steps are not available since there is no data for i_{s+1}. It could be concluded that CCS-MPC has certain features that avoid the existing issues of FCS-MPC for PV applications.

6. Conclusion

A CCS-MPC has been designed for a solar energy conversion system in order to enhance the efficiency of INC method for MPPT. The proposed controller has been applied on a DC-DC buck converter to charge up the batteries from a PV panel. Moreover, the INC algorithm has been modified to comply with the proposed controller requirements. The closed loop performance has been investigated through simulation study to compare the proposed controller with conventional PI. The simulation results show better transient dynamic and disturbance rejection performances for CCS-MPC which led to harvest higher amount of available photovoltaic power. The practical implementation of the introduced algorithm illustrated its performance for MPPT and controlling the delivered power to the energy storage system. The practical issues have been discussed and superior properties of the CCS-MPC explained against the previously reported predictive methods. It is concluded that using such technique is beneficial to have a constant switching frequency, which is mandatory in filter design. Moreover, it could increase the performance of the active switches in comparison with a FCS-MPC algorithm with varying and high switching frequency.

Appendix A. Supplementary material

Supplementary data associated with this article can be found, in the online version, at http://dx.doi.org/10.1016/j.ijepes.2018.05.004.

References

[1] Feldman D, Barbose G, Margolis R, Bolinger M, Chung D, Fu R, et al. Photovoltaic system pricing trends; 2015.

[2] Dehghanzadeh A, Farahani G. A survey on maximum power point tracking techniques in solar installations. In: Presented at the international conference on new research achievements in electrical and computer engineering, Tehran; 2016.

[3] Sher HA, Murtaza AF, Noman A, Addoweesh KE, Al-Haddad K, Chiaberge M. A new sensorless hybrid MPPT algorithm based on fractional short-circuit current measurement and P&O MPPT. IEEE Trans Sustain Energy 2015;6:1426–34.

[4] De Brito MAG, Galotto L, Sampaio LP, e Melo GdA, Canesin CA. Evaluation of the main MPPT techniques for photovoltaic applications. IEEE Trans Indus Electron 2013;60: 1156–67.

[5] Kadri R, Gaubert J-P, Champenois G. An improved maximum power point tracking for photovoltaic grid-connected inverter based on voltage-oriented control. IEEE Trans Ind Electron 2011;58:66–75.

[6] Alajmi BN, Ahmed KH, Finney SJ, Williams BW. Fuzzy-logic-control approach of a modified hill-climbing method for maximum power point in microgrid standalone photovoltaic system. IEEE Trans Power Electron 2011;26:1022–30.

[7] Al Nabulsi A, Dhaouadi R. Efficiency optimization of a DSP-based standalone PV system using fuzzy logic and dual-MPPT control. IEEE Trans Indus Inform 2012;8: 573–84.

[8] Lin W-M, Hong C-M, Chen C-H. Neural-network-based MPPT control of a stand-alone hybrid power generation system. IEEE Trans Power Electron 2011;26:3571–81.

[9] Dahmane M, Bosche J, El-Hajjaji A, Pierre X. MPPT for photovoltaic conversion systems using genetic algorithm and robust control. In: 2013 American control conference; 2013. p. 6595–600.

[10] Bordons C, Montero C. Basic principles of MPC for power converters: bridging the gap between theory and practice. IEEE Ind Electron Mag 2015;9:31–43.

[11] Wang L. Model predictive control system design and implementation using MATLAB®. Springer Science & Business Media; 2009.

[12] Rodriguez J, Kazmierkowski MP, Espinoza JR, Zanchetta P, Abu-Rub H, Young HA, et al. State of the art of finite control set model predictive control in power electronics. IEEE Trans Ind Inf 2013;9:1003–16.

[13] Vazquez S, Leon JI, Franquelo LG, Rodriguez J, Young HA, Marquez A, et al. Model predictive control: a review of its applications in power electronics. IEEE Ind Electron Mag 2014;8:16–31.

[14] Kouro S, Cortés P, Vargas R, Ammann U, Rodríguez J. Model predictive control—a simple and powerful method to control power converters. IEEE Trans Ind Electron 2009;56:1826–38.

[15] Kakosimos PE, Kladas AG. Implementation of photovoltaic array MPPT through fixed step predictive control technique. Renew Energy 2011;36:2508–14.

[16] Kakosimos PE, Kladas AG, Manias SN. Fast photovoltaic-system voltage-or current-oriented MPPT employing a predictive digital current-controlled converter. IEEE Trans Ind Electron 2013;60:5673–85.

[17] Shadmand MB, Balog RS, Abu-Rub H. Model predictive control of PV sources in a smart DC distribution system: maximum power point tracking and droop control. IEEE Trans Energy Convers 2014;29:913–21.

[18] Sajadian S, Ahmadi R. Model predictive-based maximum power point tracking for grid-tied photovoltaic applications using a Z-source inverter. IEEE Trans Power Electron 2016;31:7611–20.

[19] Leon JI, Kouro S, Franquelo LG, Rodriguez J, Wu B. The essential role and the continuous evolution of modulation techniques for voltage-source inverters in the past, present, and future power electronics. IEEE Trans Ind Electron 2016;63:2688–701.

[20] Judewicz MG, Gonzalez SA, Echeverria NI, Fischer JR, Carrica DO. Generalized predictive current control (GPCC) for grid-tie three-phase inverters.

[21] Calle-Prado A, Alepuz S, Bordonau J, Nicolas-Apruzzese J, Cortés P, Rodriguez J. Model predictive current control of grid-connected neutral-point-clamped converters to meet low-voltage ride-through requirements. IEEE Trans Ind Electron 2015;62:1503–14.

[22] Aguirre M, Kouro S, Rojas CA, Rodriguez J, Leon JI. Switching frequency regulation for FCS-MPC based on a period control approach. IEEE Trans Ind Electron 2018;65:5764–73.

[23] Tomlinson M, du Toit Mouton H, Kennel R, Stolze P. A fixed switching frequency scheme for finite-control-set model predictive control—concept and algorithm. IEEE Trans Ind Electron 2016;63:7662–70.

[24] Lezana P, Aguilera R, Quevedo D. Steady-state issues with finite control set model predictive control. In: Industrial electronics, 2009. IECON'09. 35th Annual conference of IEEE; 2009. p. 1776–81.

[25] Aguilera RP, Lezana P, Quevedo DE. Finite-control-set model predictive control with improved steady-state performance. IEEE Trans Ind Inf 2013;9:658–67.

[26] Metri JI, Vahedi H, Kanaan HY, Al-Haddad K. Real-time implementation of model-predictive control on seven-level packed U-cell inverter. IEEE Trans Ind Electron 2016;63:4180–6.

[27] Sun J, Grotstollen H. Averaged modelling of switching power converters: reformulation and theoretical basis. In: Power electronics specialists conference, 1992. PESC'92 Record., 23rd Annual IEEE; 1992. p. 1165–72.

[28] Bacha S, Munteanu I, Bratcu AI. Power electronic converters modeling and control, vol. 5, Springer; 2014.

[29] Khalil HK. Noninear systems. New Jersey: Prentice-Hall 1996;2: p. 5.1.

[30] Dehghanzadeh A, Farahani G, Maboodi M. A novel approximate explicit double-diode model of solar cells for use in simulation studies. Renew Energy 2017;103:468–77.

[31] Dehghanzadeh A, Farahani G, Vahedi H, Al-Haddad K. Explicit double-exponential modeling methods for photovoltaic cells. In: Industrial Technology (ICIT), 2017 IEEE international conference on; 2017. p. 423–8.

[32] Vahedi H, Shojaei AA, Chandra A, Al-Haddad K. Five-level reduced-switch-count boost PFC rectifier with multicarrier PWM. IEEE Trans Ind Appl 2016;52:4201–7.